Journal of Power Sources 195 (2010) 857–861

Contents lists available at ScienceDirect

Journal of Power Sources

journal homepage: www.elsevier.com/locate/jpowsour

Short communication

Converting cobalt oxide subunits in cobalt metal-organic framework into agglomerated Co_3O_4 nanoparticles as an electrode material for lithium ion battery

Bo Liu[a,b], Xinbo Zhang[a], Hiroshi Shioyama[a], Takashi Mukai[a], Tetsuo Sakai[a], Qiang Xu[a,b,*]

[a] National Institute of Advanced Industrial Science and Technology (AIST), Ikeda, Osaka 563-8577, Japan
[b] Graduate School of Engineering, Kobe University, Nada Ku, Kobe, Hyogo 657-8501, Japan

ARTICLE INFO

Article history:
Received 22 May 2009
Received in revised form 13 July 2009
Accepted 14 August 2009
Available online 28 August 2009

Keywords:
Agglomerated structure
Cobalt oxide
Lithium ion battery
Metal-organic framework
Secondary building units

ABSTRACT

Co_3O_4 nanoparticles are prepared via converting cobalt oxide subunits in a cobalt metal-organic framework ($Co_3(NDC)_3(DMF)_4$, NDC = 2,6-naphthalene- dicarboxylate; DMF = N,N′-dimethylformamide) by pyrolysis in air. The as-prepared Co_3O_4 shows an agglomerated secondary structure with an average diameter of around 250 nm comprised of small primary Co_3O_4 particles with a size of about 25 nm. This agglomerated structure favors the enhanced capacity, improved rate capability and prolonged cycle life as an electrode material for lithium ion batteries.

1. Introduction

Metal-organic frameworks (MOFs), emerging multifunctional materials, have attracted much attention due to their wide applications [1–8]. Generally, MOFs hold two features: one is secondary building units (SBUs) and the other is high porosity. Nowadays, more interests have been focused on the controls and applications of the pores in MOFs, while little attention has been paid on the application of the SBUs. Metal oxide clusters with the size in order of angstrom in MOFs can be converted into nanostructural metal oxides, which are of great importance in many applications [9–12].

Since the first report of nanosized Co_3O_4 as electrode materials for lithium ion battery (LIB) in 2000 [13], great attention has been paid to improve its electrode performance by controlling the Co_3O_4 structures and textures [14–23], because Co_3O_4 electrode can in principle deliver three times as high as the capacity of currently used graphite (<372 mAh g^{-1}). However, Co_3O_4 electrode usually suffers from poor capacity retention upon cycling and/or poor rate capability, which have been attributed to the large volume changes during the repeated lithium uptake and removal reactions and the degradation of the electrolyte on the solid-electrolyte interface (SEI) [24–26,23,27]. It is believed that directly starting from large agglomerates made of nanometric Co_3O_4 particles could provide a solution to issue the problem above [15–17]. Virus biotemplated Co_3O_4 nanowires made up of Co_3O_4 nanocrystals (2–3 nm) give rise to the improved electrochemical performance in specific capacity and rate capability as an electrode material for LIB [15]. A Co_3O_4 nanotube (diameter of 30 nm) consisting of the small nanoparticles (size of 5–10 nm) prepared by a one-step self-supported topotactic transformation approach has exhibited the superior LIB performance [16]. More recently, mesoporous single-crystal Co_3O_4 nano-needles constructed from small nanocrystals have shown very low initial irreversible loss, ultrahigh reversible capacity and excellent capacity retention over 50 cycles [27]. The increasing evidence has shown that it is an attractive way to fabricate agglomerated Co_3O_4 with varied structures and textures to improve the electrode performance for LIB. However, to date, no direct and efficient approach has been reported to fabricate such agglomerated structure due to the homogeneous reaction conditions employed in various approaches such as template syntheses [26], ALD [28], MOCVD [29], sol–gel process [30] and spray pyrolysis [31] and so on.

Herein, we, for the first time, develop a novel MOF route for preparing agglomerated Co_3O_4 nanoparticles, which involves the processes of converting metal oxide subunits in MOF into primary metal oxide nanoparticles and subsequently agglomerating into the secondary nanoparticles (Scheme 1). The resultant agglomerated Co_3O_4 nanoparticles prepared by the MOF route showed a

* Corresponding author at: National Institute of Advanced Industrial Science and Technology (AIST), 1-8-31 Midorigaoka, Ikeda, Osaka 563-8577, Japan.
Tel.: +81 72 751 9652; fax: +81 72 751 7942.
E-mail address: q.xu@aist.go.jp (Q. Xu).

0378-7753/$ – see front matter © 2009 Elsevier B.V. All rights reserved.
doi:10.1016/j.jpowsour.2009.08.058

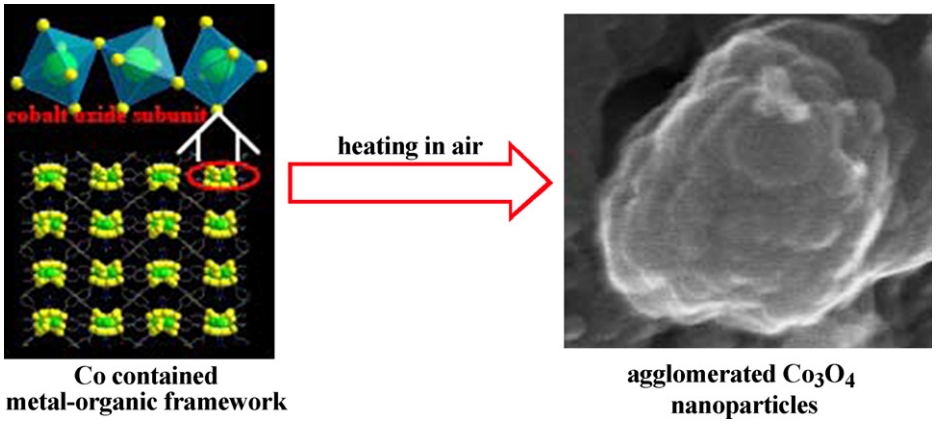

Scheme 1. Growth illustration of agglomerated Co_3O_4 nanoparticles.

reversible capacity of 965 mAh g^{-1} (86% of initial capacity) beyond 50 cycles at a current density of 50 mA g^{-1}. The excellent electrochemical performance and the facile preparation suggest practical use of agglomerated Co_3O_4 electrodes in lithium ion batteries.

2. Experimental

$Co_3(NDC)_3(DMF)_4$ (cobalt-MOF, NDC = 2,6-naphthalene-dicarboxylate; DMF = N,N′-dimethylformamide) was synthesized as described in our previous work [32]. Agglomerated Co_3O_4 nanoparticles were grown by heating $Co_3(NDC)_3(DMF)_4$ at 600 °C for 1 h in air with a heating rate of 10 °C min^{-1} (Scheme 1).

Powder X-ray diffraction (PXRD) was carried out on a Rigaku X-ray diffractometer (Rigaku Rint, Japan). TGA were performed on a Shimadzu DTG-50 thermal analyzer from room temperature to 600 °C at a heating rate of 5 °C min^{-1}. A scanning electron microscope (SEM, S-5000, Hitachi, Japan) was used to observe the morphology of as-made Co_3O_4. Transmission electron microscopic (TEM) investigations were carried out using a JEOL 3000 instrument operated at 200 kV. X-ray photoelectron spectrum (XPS) was acquired with an ESCA-3400 spectrometer (Simadzu, Japan) equipped with a Mg Kα X-ray exciting source (1253.6 eV) operating at 10 kV and 10 mA. The nitrogen sorption isothermals were measured using an automatic volumetric adsorption equipment (BEL mini, Japan).

The electrochemical properties of the as-prepared Co_3O_4 sample were examined using a two-electrode electrochemical cell. The working electrodes were prepared by a slurry coating procedure. The slurry consisted of 85 wt.% active material (as-prepared Co_3O_4), 5 wt.% black carbon and 10 wt.% polyvinylidene fluoride (PVDF) dissolved in N-methyl pyrrolidinone (NMP), and was spread on a copper mesh current collector (sample thickness = 50 μm). The mesh was dried in a vacuum oven at 150 °C for 3 h. Test cells were assembled in a dry room using Li foil as counter electrode, polypropylene (PP) film as separator. The electrolyte was 1.0 M $LiPF_6$ in a 50:50 (w/w) mixture of ethylene carbonate (EC) and diethyl carbonate (DEC). The assembled cells were galvanostatically cycled between 3.0 and 0.01 V versus Li/Li^+ at 20 °C.

3. Results and discussions

Synthesis, structure and characteristics of $Co_3(NDC)_3(DMF)_4$ (cobalt-MOF, NDC = 2,6-naphthalene dicarboxylate; DMF = N,N′-dimethylformamide) have been described in our previous work [32]. The secondary building units (SBUs) in this MOF contain a linear cobalt oxide subunit (dimensions, 4 Å × 4 Å × 11 Å) [32,33]. As shown in the TG curve of the cobalt-MOF in the atmosphere of air (Fig. 1a), the first step of weight loss (24.7%) takes place between 130 and 300 °C, which corresponds to the removal of the coordinated DMF molecules (calc. 24.1%). The subsequent heating results in the complete decomposition of metal-organic framework at the temperature above 400 °C with a cliffy weight loss in TG curve. In the present case, the Co_3O_4 subunits content in cobalt metal-organic framework ($Co_3(NDC)_3DMF_4$, $C_{48}H_{46}Co_3N_4O_{16}$) is calculated to be 21.7 wt.%, which is very close to the Co_3O_4 content (23.4 wt.%) determined by thermogravity analysis performed in a Ar flow. The small deviation may be attributed to the guest molecules or air moisture adsorbed/desorbed by cobalt metal-organic framework. Fig. 1b shows the PXRD pattern of cobalt-MOF sample after heating at 600 °C in air, where all the peaks are ascribed to the Co_3O_4 phase (JCPDS card no. 42-1467) and no other phases such as CoO and Co_2O_3 can be identified. The sharp peaks indicate that the as-prepared Co_3O_4 sample is highly crystalline. When the cobalt-MOF is heated at 600 °C in an inert atmosphere (Ar flow),

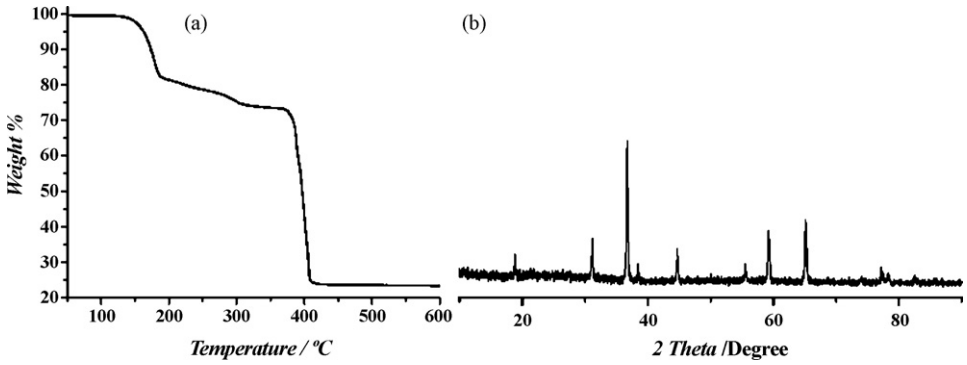

Fig. 1. (a) TG curve of cobalt-MOF with a heating rate of 5 °C min^{-1} in air and (b) PXRD pattern of as-prepared Co_3O_4.

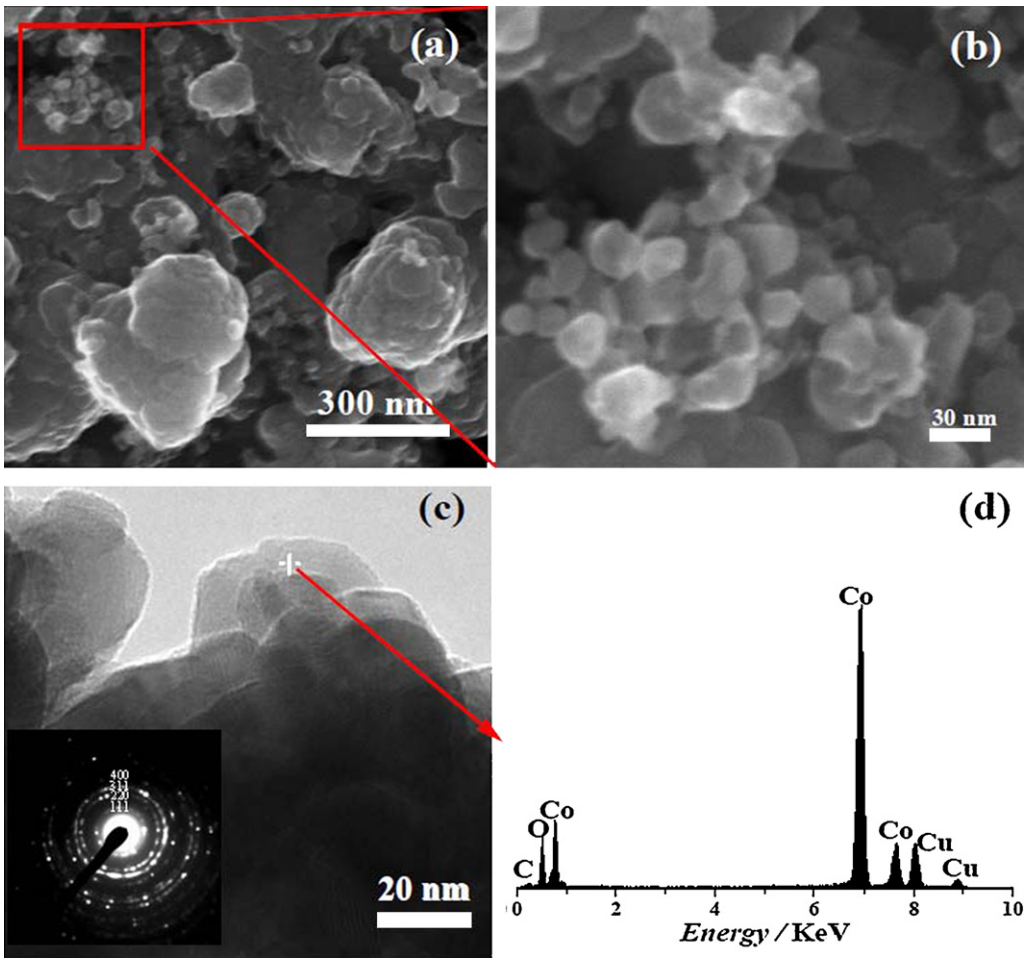

Fig. 2. (a) SEM images of the as-prepared Co_3O_4 and (b) enlarged region in (a), showing the characteristic of primary nanoparticles; (c) TEM image (inset: SAED image) and (d) EDS of the as-prepared Co_3O_4.

however, the final sample is assigned to the mixed phases of Co and CoO according to the PXRD analysis [33]. It is clear that cobalt oxide subunits in cobalt-MOF are converted into Co_3O_4 by heating at 600 °C in air. Energy dispersive X-ray spectroscopy (EDS) (Fig. 2d) and X-ray photoelectron energy spectrum (XPS) analyses [33] also confirm that the final product can be identified to Co_3O_4. The carbon and copper signals are originated from the Cu-mesh supporting the TEM sample in EDS. More structural details of the as-prepared Co_3O_4 sample have been investigated by means of SEM and TEM as shown in Fig. 2. Agglomerated nanostructures of the Co_3O_4 can be observed in SEM images, in which large particles with average size around 250 nm are comprised of the small particles with size of about 25 nm in a densely stacking style (Fig. 2a and b). The densely stacking style of Co_3O_4 nanoparticles is also confirmed in TEM observation, in which the sizes of small particles agree with the SEM observation. The surface area of as-prepared Co_3O_4 is determined to be 5.3 $m^2\,g^{-1}$ by Brunauer–Emmett–Teller (BET) method [33]. The theoretically calculated surface areas taking the particle diameters of 25 and 250 nm are 39.3 and 3.93 $m^2\,g^{-1}$, respectively ($S = 6/d\rho$, d is the particle diameter; ρ is the density, 6110 kg m^{-3}). The comparison of experimental and calculated surface area suggests that separated small nanoparticles are of low ratio. Associated with the electronic microscopic observations, we can conclude that most small particles stacked tightly into large agglomerated structures. The crystalline nature of the as-prepared Co_3O_4 is also conformed in the selected area electron diffraction (SAED) pattern (Fig. 2c, inset), which is consistent with the PXRD analysis.

The MOF route for preparing Co_3O_4 is much different from other conventional methods, which are favorable for the formation of uniformly separated micrometric or nanometric particles due to the homogeneous reaction conditions [26,28–31]. In contrast, the agglomerated structures can be obtained by the MOF route. Metal oxide subunits (sizes in order of angstrom) in MOF are converted into tiny metal oxide clusters by heating, which re-crystallize to primary nanoparticles. The primary nanoparticles from neighboring MOF crystals are then agglomerated into the larger secondary micrometric or nanometric structures with a dense stack fashion, as identified by the SEM and TEM observations.

To test the idea that an electrode with agglomerated structure is advantageous for LIB, the electrochemical performance of the as-prepared agglomerated Co_3O_4 nanoparticles is evaluated by a standard Co_3O_4/Li coin type half cell. Fig. 3a shows the charge/discharge curves of the as-prepared Co_3O_4 in Li-ion test cell at a current density of 50 mA g^{-1} and a temperature of 20 °C. During the first discharge, the potential of Co_3O_4 electrode quickly falls to about 1.1 V with a long plateau which is associated with the reduction of Co_3O_4 into Co and then declines to the cut-off voltage of 0.01 V. A high discharge capacity (1118 mAh g^{-1}) is produced during the first discharge process. The initial capacity retention reaches up to 75% in the first cycle. Interestingly, the capacity exhibits a gradual increase in subsequent cycles to a highest value of 965 mAh g^{-1} at 50th cycles (Fig. 3b), which is 86% of the initial capacity. This feature may be attributed to the unique structural characteristic of the agglomerated Co_3O_4. Mesoporous Co_3O_4 prepared from a hard template route and mesoporous

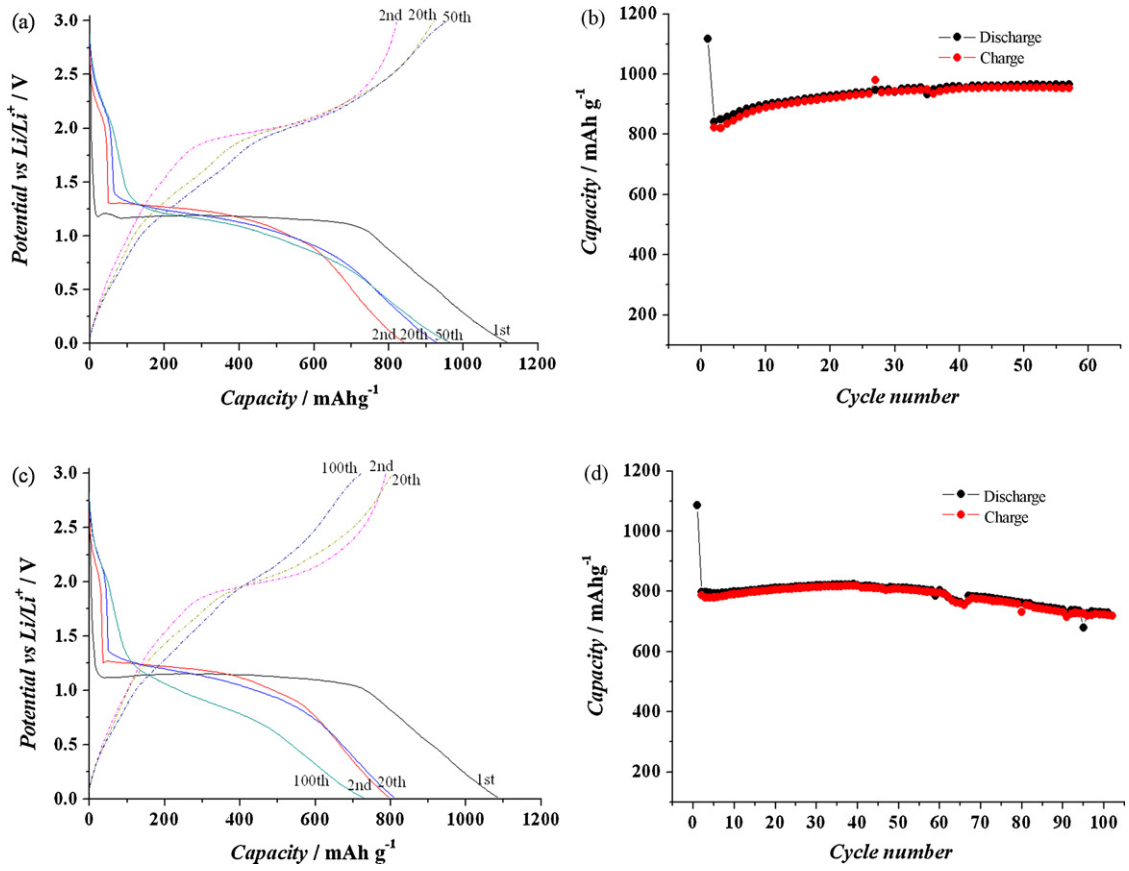

Fig. 3. (a) Charging–discharging curves and (b) cycle performance at a current density of 50 mA g^{-1}; (c) charging–discharging curves and (d) cycle performance at a current density of 100 mA g^{-1} for the as-prepared Co_3O_4/Li half cell cycled between 3.0 and 0.01 V. Only the mass of Co_3O_4 was considered for calculating the specific capacity.

single-crystal Co_3O_4 nano-needles obtained from thermal oxidative decomposition of β-$Co(OH)_2$ nano-needles exhibit similar electrochemical behavior [26,29]. As demonstrated, the rigid structure favors improved cycling performance (>50 cycles) [27], which is consistent with our experimental results supported by agglomerated Co_3O_4 structure with densely stacking style. In contrast, only 550 mAh g^{-1} of capacity remains for Co_3O_4 microsphere prepared by hydrothermal reaction after 25 cycles at a current density of 50 mA g^{-1} [34]. It has been claimed that the Co_3O_4 nanotubes with diameter of 30 nm consisting of small Co_3O_4 nanoparticles with size of 5–10 nm gives rise to the best performance for Co_3O_4-based anode materials for lithium ion batteries. Although the capacity is high (1200 mAh g^{-1}), the retention of the initial capacity is low (62%) and the reported cycle life is short (20 cycles) [16]. For the needle-like Co_3O_4 nanotubes prepared by self-supported topotactic transformation approach, the capacity is declined to lower than 400 mAh g^{-1} after 80 cycles at a current density of 50 mA g^{-1} [19]. To evaluate the rate capability of the agglomerated Co_3O_4 electrode, the cycle performance was also tested at a higher current density of 100 mAh g^{-1}. It shows a similar behavior with that measured at the current density of 50 mA g^{-1} (Fig. 3c and d). The capacity in the first discharge is 1090 mAh g^{-1}, 730 mAh g^{-1} of which remains beyond 100 cycles with a highest value of 824 mAh g^{-1} at 39th cycle (Fig. 3d). It is clear that the agglomerated Co_3O_4 nanocrystalline favors the superior electrochemical performance as electrode materials for LIB due to its unique primary-secondary agglomerated structure. Li et al. attribute the high capacity and rate capability of the nanowires (NW) electrodes to the unique hierarchical architecture [18]. As described in their paper, the porosity of NW electrode will enhance the electrolyte/Co_3O_4 contact area, shorten the Li^+ ion diffusion length in the NWs and accommodate the strain induced by the volume change during the electrochemical reaction. However, Co_3O_4 electrode material with the highest BET surface area reported by Lou et al. displays the worst electrochemical performance for lithium batteries among their three samples prepared by thermal decomposition and re-crystallization of precursor β-$Co(OH)_2$ nano-needles [27]. In our present case, although the Co_3O_4 electrode material has a small BET surface area, it shows high capacity and excellent cyclical stability. The good cycle performance of Co_3O_4 electrodes might be associated with the stability of solid-electrolyte interface (SEI), although its mechanism is not yet clear. We speculate the enhanced electrochemical performance of Co_3O_4 electrode is due to their unique primary-secondary agglomerated structure. Associated with the simplicity in preparation, it will be excellent candidate as electrode materials for next-generation LIB.

It is noteworthy that electrode performance of MOFs themselves is very poor and many attempts aimed at using MOFs as Li-based energy storage materials failed [35–37], due to the insulating nature of MOFs. Recently, the electrochemical performance has been improved with a mixed-valence MOF as an electrode material [38]. However, the lithium storage capability is very low (75 mAh g^{-1}), owing to the limited number of inserted Li atoms per formula and the low density of the mixed-valence MOF. By a simple pyrolysis process reported in this work, the product obtained from MOF with poor electrode performance gives rise to much superior electrochemical performance.

4. Conclusions

In summary, we have, for the first time, developed a MOF route for synthesizing agglomerated Co_3O_4 nanoparticles with the diam-

eter of around 250 nm consisting of the small nanoparticles with the size of about 25 nm by converting cobalt oxide subunits in a cobalt-MOF via pyrolysis. This agglomerated Co_3O_4 favors the enhanced capacity, improved rate capability and prolonged cycle life as an electrode material for LIB. It is feasible to improve the Co_3O_4 electrode performance for LIB by controlling agglomerated structures with varied primary and secondary particle sizes. This work also offers us a novel perspective to exploit the potential application of fast growing MOF family.

Acknowledgements

We thank the reviewers for valuable suggestions and AIST and Kobe University for the financial support. B. Liu thanks MEXT for Japanese Government Scholarship.

Appendix A. Supplementary data

Supplementary data associated with this article can be found, in the online version, at doi:10.1016/j.jpowsour.2009.08.058.

References

[1] H. Li, M. Eddaoudi, M. O'Keeffe, O.M. Yaghi, Nature 402 (1999) 276–279.
[2] B. Chen, M. Eddaoudi, S.T. Hyde, M. O'Keeffe, O.M. Yaghi, Science 291 (2001) 1021–1023.
[3] L. Pan, B. Parker, X.Y. Huang, D.H. Olson, J.-Y. Lee, J. Li, J. Am. Chem. Soc. 128 (2006) 4180–4181.
[4] R.Q. Zou, H. Sakurai, Q. Xu, Angew. Chem. Int. Ed. 45 (2006) 2542–2546.
[5] R.Q. Zou, H. Sakurai, S. Han, R.Q. Zhong, Q. Xu, J. Am. Chem. Soc. 129 (2007) 8402–8403.
[6] K.L. Mulfort, J.T. Hupp, J. Am. Chem. Soc. 129 (2007) 9604–9605.
[7] F. Schröder, D. Esken, M. Cokoja, M.W.E. van denBerg, O.I. Lebedev, G.V. Tendeloo, B. Walaszek, G. Buntkowsky, H.-H. Limbach, B. Chaudret, R.A. Fischer, J. Am. Chem. Soc. 130 (2008) 6119–6130.
[8] B. Liu, H. Shioyama, T. Akita, Q. Xu, J. Am. Chem. Soc. 130 (2008) 5390–5931.
[9] C. Burda, X. Chen, R. Narayanan, M.A. El-Sayed, Chem. Rev. 105 (2005) 1025–1102.
[10] K.B. Zhou, X. Wang, X.M. Sun, Q. Peng, Y.D. Li, J. Catal. 229 (2005) 206–212.
[11] N. Tian, Z.Y. Zhou, S.G. Sun, Y. Ding, Z.L. Wang, Science 316 (2007) 732–735.
[12] R. Si, M. Flytzani-Stephanopoulos, Angew. Chem. Int. Ed. 47 (2008) 2884–2887.
[13] P. Poizot, S. Laruelle, S. Grugeon, L. Dupont, J.-M. Tarascon, Nature 407 (2000) 496–499.
[14] W.-Y. Li, L.-N. Xu, J. Chen, Adv. Funct. Mater. 15 (2005) 851–857.
[15] K.T. Nam, D.-W. Kim, P.J. Yoo, C.-Y. Chiang, N. Meethong, P.T. Hammond, Y.-M. Chiang, A.M. Belcher, Science 312 (2006) 885–888.
[16] N. Du, H. Zhang, B. Chen, J. Wu, X. Ma, Z. Liu, Y. Zhang, D. Yang, X. Huang, J. Tu, Adv. Mater. 19 (2007) 4505–4509.
[17] G. Binotto, D. Larcher, A.S. Prakash, R.H. Urbina, M.S. Hegde, J.-M. Tarascon, Chem. Mater. 19 (2007) 3032–3040.
[18] Y. Li, B. Tan, Y. Wu, Nano Lett. 8 (2008) 265–270.
[19] X.W. Lou, D. Deng, J.Y. Lee, J. Feng, L. Archer, Adv. Mater. 20 (2008) 258–262.
[20] X.W. Lou, L.A. Archer, Z. Yang, Adv. Mater. 20 (2008) 3987–4019.
[21] Z. Yuan, F. Huang, C. Feng, J. Sun, Y. Zhou, Mater. Chem. Phys. 79 (2003) 1–4.
[22] D. Larcher, G. Sudant, J.-B. Leriche, Y. Chabre, J.-M. Tarascona, J. Electrochem. Soc. 149 (2002) A234–A241.
[23] S.A. Needham, G.X. Wang, K. Konstantinov, Y. Tournayre, Z. Lao, H.K. Liu, Electrochem. Solid State Lett. 9 (2006) A315–A319.
[24] Y. Yu, C.H. Chen, J.L. Shui, S. Xie, Angew. Chem. Int. Ed. 44 (2005) 7085–7089.
[25] Y.M. Kang, M.S. Song, J.H. Kim, H.S. Kim, M.S. Park, J.Y. Lee, H.K. Liu, S.X. Dou, Electrochim. Acta 50 (2005) 3667–3673.
[26] K.M. Shaju, F. Jiao, A. Debar, P.G. Bruce, Phys. Chem. Chem. Phys. 9 (2007) 1837–1842.
[27] X.W. Lou, D. Deng, J.Y. Lee, L. Archer, J. Mater. Chem. 18 (2008) 4397–4401.
[28] M. Rooth, E. Lindahl, A. Harsta, Chem. Vap. Depos. 12 (2006) 209–213.
[29] M. Burriel, G. Garcia, J. Santiso, A. Abrutis, Z. Saltyte, A. Figueras, Chem. Vap. Depos. 11 (2005) 106–111.
[30] M.S. Selim, J. Cryst. Growth 265 (2004) 115–120.
[31] L.D. Kadam, P.S. Patil, Mater. Chem. Phys. 68 (2001) 225–232.
[32] B. Liu, R.-Q. Zou, R.-Q. Zhong, S. Han, H. Shioyama, T. Yamada, G. Maruta, S. Takeda, Q. Xu, Micropor. Mesopor. Mater. 111 (2008) 470–477.
[33] See supporting information.
[34] Y. Liu, C. Mi, L. Su, X. Zhang, Electrochim. Acta 53 (2008) 2507–2513.
[35] P. Tran-Van, K. Barthelet, M. Morcrette, M. Herlem, J.M. Tarascon, A.K. Cheetham, G. Férey, J. New Mater. Electrochem. Syst. 6 (2003) 29–31.
[36] C.Y. Cheng, S.J. Fu, C.J. Yang, W.H. Chen, K.J. Lin, G.H. Lee, Y. Wang, Angew. Chem. Int. Ed. 42 (2003) 1937–1940.
[37] X. Li, F. Cheng, S. Zhang, J. Chen, J. Power Sources 160 (2006) 542–547.
[38] G. Férey, F. Millange, M. Morcrette, C. Serre, M.-L. Doublet, J.-M. Grenéche, J.-M. Tarascon, Angew. Chem. Int. Ed. 46 (2007) 3259–3263.